 https://doi.org/10.3311/PPci.21309

Periodica Polytechnica Civil Engineering, 67(4), pp. 1214–1233, 2023

Experimental and Numerical Study on RC Beams Strengthened by NSM Using CFRP Reinforcements

Abderrahmane Abdesselam[1*], Abdelghani Merdas[1], Bruno Fiorio[2], Nasr-Eddine Chikh[3]

[1] Department of Civil Engineering, Emerging Materials Research Unit, University of Setif 1, Setif, 19000, Algeria
[2] Department of Civil Engineering, CY Cergy Paris University, Paris, 95011, France
[3] Department of Civil Engineering, University of Constantine 1, Constantine, 25000, Algeria
[*] Corresponding author, e-mail: abdesselam.abderrahmane@univ-setif.dz

Received: 11 October 2023, Accepted: 24 June 2023, Published online: 24 July 2023

Abstract

Near Surface Mounted (NSM) Carbon Fiber-Reinforced Polymer (CFRP) reinforcement technique to improve the flexural strength of reinforced concrete members has become increasingly attractive in recent years. In this study, the practical problem of concrete cover depth cutting limitation was investigated. Twelve specimens were tested by four-point bending until failure. Experimental parameters include concrete cover depth, CFRP reinforcement type, CFRP positioning, and stirrups status. Furthermore, a nonlinear FEA model was developed to simulate the tested beams and was able to predict the experimental behavior satisfactorily. A series of parametric studies were then performed using this model to understand the effect of various reinforcement parameters on the flexural performance of the beam. The results showed that Strengthening with CFRP resulted in a significant increase in yield and ultimate strengths, but a significant ductility loss was recorded due to CFRP strip debonding in the strengthened beams, this problem was addressed by using more efficient strengthening techniques utilizing the effective bond length and a proper groove depth and positioning for the NSM bars.

Keywords

CFRP, RC-beams, NSM, experimental, FEA, parametric study

1 Introduction

Damage to reinforced structures can be a result of inadequate reinforcement, excessive deflection, inadequate concrete quality, corroded reinforcement, or insufficient bearing capacity. [1]. All of these factors can cause cracks in structural elements. The propagation of the crack and the depth of the crack indicates the degree of damage. Amongst the different strengthening techniques that have been developed and applied to strengthen damaged RC structures, the use of fiber-reinforced polymers (FRP) reinforcements has significantly increased recently. Externally bonded FRP strips and sheets have been the most commonly used techniques for strengthening bridges and concrete structures. Numerous tests have shown that brittle fracture due to delamination of FRP and concrete cover separation was the dominating failure mode [2], so the full tensile strength of the FRP could not be utilized. The issue of premature failure in EBR systems can be addressed by utilizing near-surface mounted CFRP systems, which offer a reliable and sustainable solution for reinforcing concrete structures. These systems have been proven to effectively and efficiently improve the performance of concrete structures by expanding the interface between the FRP and concrete, leading to enhanced bonding and increased strength. The bond between NSM FRP strip/rod and concrete, have an important role in developing the interface, was analyzed mainly with beam pullout tests [3, 4]. The effectiveness of the NSM technique stems from the relatively high bonding performance between the FRP bars and the concrete substrate. Efficiency is even higher when these bars have a rectangular cross-section because they provide a larger surface area for bonding with the surrounding concrete [5–7]. Tests on simply supported RC members reinforced with NSM CFRP bars/rods have shown that these bars debond at much higher stresses compared to the EBR CFRP reinforcement technique [8, 9]. In contrast to EBR, NSM reinforcement does not require the surface of the concrete to be roughened or shot-blasted in order to ensure proper bonding between the FRP reinforcement

Cite this article as: Abdesselam, A., Merdas, A., Fiorio, B., Chikh, N.-E. "Experimental and Numerical Study on RC Beams Strengthened by NSM Using CFRP Reinforcements", Periodica Polytechnica Civil Engineering, 67(4), pp. 1214–1233, 2023. https://doi.org/10.3311/PPci.21309

and the concrete substrate and provides additional protection against environmental impacts and disruptive behavior which can compromise the durability and performance of concrete structures. Beam sample test results show that the application of the NSM FRP strip/rod significantly improved the flexural strength and stiffness of the beam [10–12]. Furthermore, the failure of beams strengthened with externally bonded FRP strips was observed with a load level significantly lower than the ultimate load measured for beams strengthened with NSM FRP reinforcing bars or strips [13]. Many studies were dedicated to investigating the bond performance of NSM FRP reinforcement showing that carbon plates have a better bond performance than steel bars, also increasing the concrete strength improves significantly the pullout forces [14–16]. In addition, increasing the roughness of the surface resulted in better bond performance [17]. To fully evaluate the effect of different strengthening parameters on the performance of reinforced concrete members, a numerical investigation is necessary to simulate the experimental results. Several researchers have conducted numerical investigations to simulate the behavior of NSM FRP retrofitted structures. Lundqvist et al. [18] analyzed the anchorage length of NSM FRP bars used for flexural strengthening of RC beams using a 3D nonlinear FEA model. Vasquez and Seracino [19] simulated the stress distributions near one of the two ends of CFRP strips in RC beams strengthened with NSM CFRP strips. Barros et al. [20] used the FEA program FEMIX to simulate the behavior of NSM CFRP strengthened columns. However, these studies used a perfect bond-slip model which may not be accurate to predict the debonding failure mode. In contrast, Obaidat et al. [21] used the cohesive zone approach to model externally bonded CFRP retrofitted beams, which can provide a more accurate prediction of debonding. Hawileh [22] developed a model using the FE program ANSYS to study the effect of different NSM material bar types and diameters. Rezazadeh et al. [23] simulated the combined effect of both EBR and NSM systems using a 3D FE model developed with the FE program ABAQUS. Hosen et al. [24] Studied the effect of using the side near surface method SNSM as an alternative to the NSM technique on the flexural behavior of RC beams. Movahedi Rad et al. [25] introduced an innovative numerical optimization to control the plastic behavior of reinforced concrete haunched beams. Khaleel Ibrahim and Movahedi Rad [26, 27] applied an optimal reliability-based design approach to reinforce concrete haunched beams and CFRP-strengthened beams. Taking into account the probabilistic nature of concrete properties and complementary strain energy values. Szép et al. [28] utilized reliability analysis to model reinforced concrete beams at elevated temperatures. Although some interesting experimental and numerical studies have been developed, the structural behavior of damaged RC elements strengthened with NSM FRP strip/rod still needs to be fully investigated. In particular, the limitation of groove cutting depth in NSM CFRP reinforcement is closely associated with the depth of concrete cover and requires careful consideration and planning to ensure effective reinforcement and long-term performance of the structure. To overcome this practical problem, this research proposes two different approaches for NSM reinforcement. In the first one, the debonding problem is improved by increasing groove sizes by slightly cutting the lower part of stirrups without damaging the main reinforcing rods. The other method of NSM reinforcement is to partially insert the CFRP strip, the exposed part is covered afterward by a layer of concrete epoxy for protection. Numerical results validated by the Experimental work obtained from four-point bending tests were used to conduct a series of parametric studies to understand the effect of various reinforcement parameters on the behavior of the beams. The paper is structured as follows: After the introduction, Section 2 offers a comprehensive explanation of the experimental program, outlining the specific procedures and methods employed, the materials utilized, and the specific setup of the experiments. Moving on to Section 3, the numerical modeling techniques utilized to analyze the beams under investigation are discussed. Section 4 is dedicated to presenting the results and discussions derived from the experiments and numerical simulations. Additionally, this section includes the validation of the numerical model against the experimental data. Furthermore, Section 5 focuses on the parametric studies conducted within this study, exploring the effects of various parameters on the structural behavior of the beams. Finally, in Section 6, the conclusions drawn from the research are presented.

2 Experimental program

2.1 Materials

2.1.1 Concrete

The concrete specimens were prepared using a mixture of Ordinary Portland Cement, fine sand (0–4 mm), crushed gravel (4–10 mm), and (6–20 mm) aggregates according to the mix proportion presented in Table 1. After casting, the specimens were cured in water (20C) for a duration

Table 1 Mix proportion of concrete

Water l/m³	Cement kg/m³	Sand kg/m³	Gravel 4/10 kg/m³	Gravel 6.3/20 kg/m³	W/C	G/C
209	336	419	471	834	0.62	2.48

of 28 days. To evaluate the hardened concrete properties, compression tests were conducted on (160 mm × 320 mm) specimens, in accordance with the NF P 18-406 standard [29]. Tensile strength *f*ct was measured using splitting tests as per the NF P 18-408 standard [30]. The average values of the three characterization cylinders tested were considered to determine the properties of concrete.

The results revealed that the average compressive strength of the concrete was 33.76 MPa, while the average tensile strength and modulus of elasticity were 3.11 MPa and 33.55 GPa, respectively.

2.1.2 Steel reinforcements

The study employed high-grade steel bars with an 8 mm diameter as the primary longitudinal reinforcements, along with mild steel bars with a 6 mm diameter for transverse stirrups. The properties of the steel reinforcement were experimentally determined in accordance with Euro-Norm EN10002 [31] with the average values obtained from testing three specimens.

2.1.3 CFRP reinforcements

To assess the tensile strength and Young's modulus of the CFRP materials used in the study, three specimens were cut to a length of 440 mm and connected to a hydraulic tensile machine through custom-made steel tubes measuring 25 cm in length and 12 mm in diameter. The CFRP rod had a circular cross-section with a diameter of 8 mm, while the CFRP strip had a rectangular cross-section measuring 20 mm in width and 2.5 mm in thickness. Uniaxial tensile tests were conducted in accordance with Euro-Norm EN10002 [31] using a load-control mode with a constant rate of 0.1 kN/s until the reinforcement failed.

2.1.4 Epoxy adhesive

To fill the grooves, EPONAL 371 epoxy adhesive was used. To determine its tensile strength and modulus of elasticity, standard Tensile Tests were conducted in accordance with ISO 527-1 specifications [32]. Ten Dog-bone-shaped specimens, each measuring 170 mm in length and with a cross section of 20 mm × 4 mm, were prepared according to ISO 527-2 [33]. The tests were conducted using a 30-kN electro-mechanical testing machine equipped with an extensometer (5 mm) to measure deformation of the Samples. The tests were carried out in a displacement control mode with a constant displacement rate of 0.01 mm/min. Material properties determined from the tests are summarized in Table 2.

2.2 Specimen configuration

The experimental study involved twelve (12) concrete beam specimens initially reinforced with steel bars for their flexural strength. To enhance their flexural capacity, CFRP-NSM strengthening scheme was employed. All twelve beams were 1000 mm long and had a rectangular cross-section of 150 mm in height and 100 mm in width. For the flexural reinforcement, two 8 mm diameter bars were used for tension and compression reinforcement, which satisfied a steel ratio of 0.0067. To prevent shear failure from occurring prior to flexural failure, rectangular stirrups made of 6 mm diameter were placed at

Table 2 Material properties

Material	Property	Standard deviation		CV %
Concrete	Compressive strength (MPa)	33,76	1,33	3,94
	Tensile strength (MPa)	3,18	0,36	11,35
	Modulus of elasticity (GPa)	33.55	1.39	4.14
Compression and tension steel reinforcement	Diameter (mm)	8	/	/
	Tensile strength (MPa)	666.20	10.71	1.60
	Yield stress (MPa)	598.1	8.25	1.37
	Modulus of elasticity (GPa)	200	/	/
Sear steel stirrup	Diameter (mm)	6	/	/
	Tensile strength (MPa)	558.91	26.58	2.25
	Yield stress (MPa)	456.19	12.16	2.66
	Modulus of elasticity (GPa)	200	/	/
CFRP rod	Diameter (mm)	8	/	/
	Tensile strength (MPa)	2561.23	36.98	1.44
	Modulus of elasticity (GPa)	179.46	1.52	0.84
CFRP strip	Thickness × width (mm)	2.5 × 20	/	/
	Tensile strength (MPa)	2538.15	157.79	6.2
	Modulus of elasticity (GPa)	179.85	0.78	0.44
Epoxy resin	Tensile strength (MPa)	31,7	3.2	10.09
	Modulus of elasticity (MPa)	3800	130	3.42
	Ultimate strain (%)	1.2	0.1	8.33

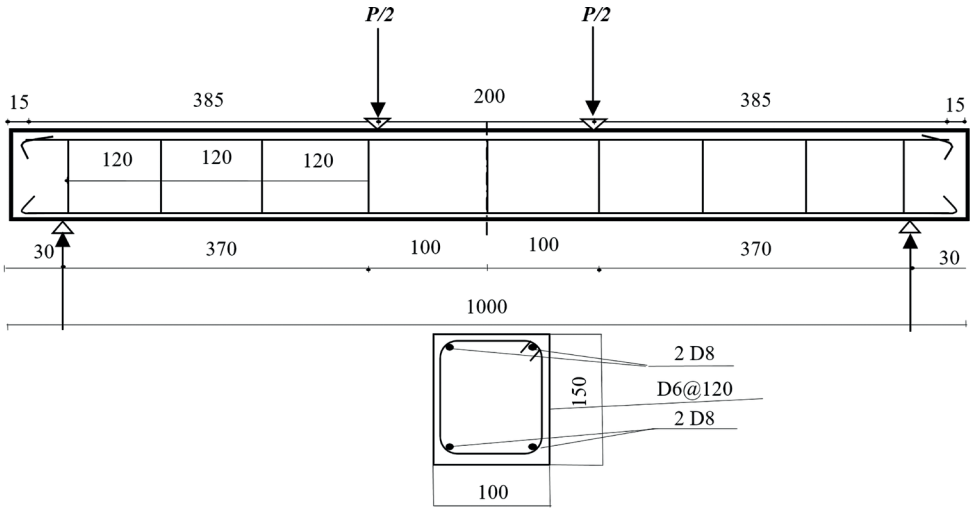

Fig. 1 Details and cross section of the specimen (mm)

every 120 mm in the shear zone. The geometric dimensions and reinforcing details of the typical beam specimen prior to the strengthening process are illustrated in Fig. 1.

2.3 Test parameters

Table 3 provides an overview of the experimental parameters considered in the study. To establish a basis for comparison, control specimens were also cast alongside the tested beams. The experimental variables include the type of reinforcement (rod or strip), depth of concrete cover (10 mm or 30 mm), method of CFRP strip insertion (full or partial), and state of shear stirrups (unaltered or partially cut at the bottom) as shown in Fig. 2. All strengthened beams shared a similar CFRP reinforcement ratio, ensuring consistency in the experimental setup. The specimen names were assigned based on specific characteristics: (C) denoted control beams, while (B) indicated upgraded beams. (10 or 30) indicated the concrete cover depth, type of CFRP reinforcement (R for rod, S for strip). Furthermore, the CFRP strip embedment was designated as (F for full or P for partial), while the state of shear stirrups was indicated by (1) for unchanged or (2) for partially cut.

Table 3 Experimental parameters

Designation of specimens	Number of specimens	CFRP Reinforcement	Concrete cover (mm)
C10	2	Without	10
C30	2	Without	30
B30RF1	2	CFRP rods fully embedded	30
B30SF1	2	CFRP strip fully embedded	30
B10SP1	2	CFRP strip partially embedded	10
B10SF2	2	CFRP strip fully embedded with cutting off steel stirrups at bottom	10

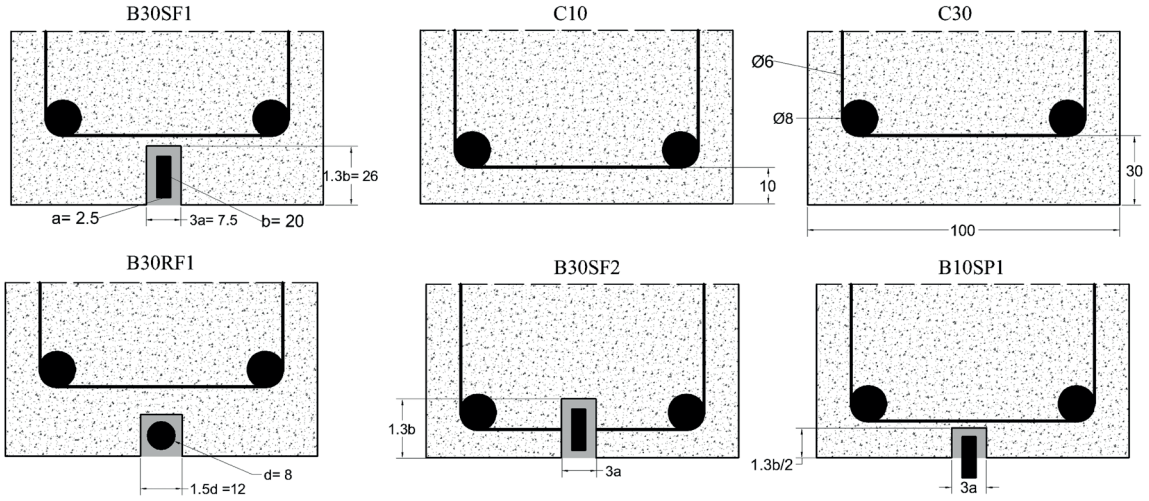

Fig. 2 Test variables

(a) (b) (c)

Fig. 3 Strengthening procedure (a) Steel reinforcements assembling, (b) Concrete misture pouring, (c) Groove cutting, placing of CFRP bars and epoxy filling

2.4 Strengthening method

Fig. 3 illustrates the key steps involved in applying the NSM CFRP strengthening method. The process begins by creating grooves in the concrete cover on the tension surface of the beam. To facilitate the groove cutting, the specimens were cured for 28 days and then rotated 180°. A diamond blade saw was used to cut the grooves, which were approximately 12 mm wide and 15 mm deep for rod reinforcement and 7.5 mm wide and 26 mm (or 13 mm) deep for strip reinforcement. The length of each groove was set at 750 mm, which is 80% of the net span for all specimens. Once the grooves were cut, they were cleaned, and compressed air was used to remove any debris and fine particles to ensure a proper bond between the adhesive epoxy and the concrete. Next, each groove was half-filled with adhesive epoxy, and the CFRP rod or strip was inserted and lightly pressed to displace the epoxy. The groove was then filled with more paste, the surface was leveled, and any excess adhesive was removed. After the NSM strengthening was complete, the specimens were cured for 3 days to allow the epoxy adhesive to reach its designed strength, after which flexural tests were conducted.

2.5 Loading and measurement methods

All twelve beam specimens were subjected to four-point loading to failure using an INSTRON machine with a capacity of 250 kN. The loading was applied under displacement control at a speed of 1.0 mm/min until failure. Test data was recorded by a static data logger and a computer at intervals of 1 second. The displacement at the center of the specimen during loading was measured by linear variable differential transformers (LVDTs) located at mid-span. Additionally, electrical resistance strain gauges were positioned on the FRP reinforcement at the mid-span's bottom to accurately measure strain levels throughout the loading process. To ensure accurate and reliable data collection, an automated data logging system was employed during the experimental procedure. This system recorded essential parameters such as load, displacement, and strain measurements at each stage of loading.

3 Numerical simulation

To simulate the behavior of the NSM CFRP reinforced beams, a three-dimensional finite element modeling of the strengthened specimens is carried out using the FEA software ABQSUS numerical results of the load-deflection curves, strain, and cracking pattern were compared with the experimental ones.

3.1 Description of the finite element model

To reduce computational time and allow for finer meshing, only a quarter of the beam was modeled by taking advantage of the geometry, loading, and boundary condition symmetries. 3D solid deformable elements (C3D8R) were utilized to simulate the concrete, CFRP strips, and epoxy adhesive, while 3D truss elements (T3D2) embedded in concrete were employed to model the steel reinforcement bars and stirrups. Cohesive elements (COH3D8) were adopted to simulate the interface between adhesive/CFRP/concrete. Sensitivity analysis was conducted to verify the mesh dimensions and assess their impact on accuracy and calculation time. The analysis revealed that the most optimal results were obtained with a mesh size of 10 mm for the concrete beam. In areas of importance and locations where relatively high strain gradients were anticipated, a finer mesh was assigned. Additionally, a mesh size of 4 mm was chosen for the epoxy and CFRP reinforcement. The support and loading conditions were simulated based on the experimental setup as depicted in Fig 4.

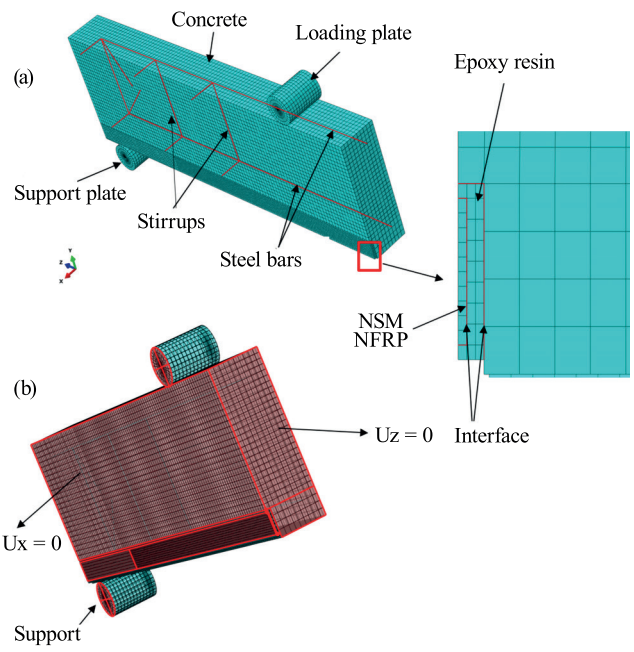

Fig. 4 (a) Meshed FE model, (b) boundary conditions

3.2 Materials modeling

Several concrete modeling approaches have been developed recently, and in this study, the concrete damaged plasticity (CDP) model was used to simulate the nonlinear behavior of concrete. The CDP model assumes two main failure mechanisms: cracking formation and propagation in tension and concrete crushing in compression [34]. Following a sensitivity analyses, the calibrated CDP parameters necessary for defining in Abaqus are: dilation angle (ψ = 38°), eccentricity (ξ = 0.1), the ratio of initial equibiaxial compressive yield stress to initial uniaxial compressive yield stress (σ_{b0}/σ_{c0}) = 1.16, the ratio of the second stress invariant on the tensile meridian to that on the compressive meridian (K = 0.667).

The CDP data, which includes the compressive crushing and tensile cracking, were calculated based on the mechanical properties of the tested specimens (Table 2) as follows: The stress-strain relationship utilized for modeling the nonlinear behavior of concrete under uniaxial compression was proposed by Carreira and Chu [35] and is described by Eq. (1) and Eq. (2).

$$\frac{\sigma}{f_{cm}} = \frac{\beta_c(\varepsilon/\varepsilon_c)}{\beta_c - 1 + (\varepsilon/\varepsilon_c)^{\beta_c}}, \tag{1}$$

$$\beta_c = \left(\frac{f_{cm}}{32.4}\right)^3 + 1.55(\text{MPa}), \tag{2}$$

where σ is the section's normal stress, f_{cm} is the mean compressive concrete strength, β_c is the form factor of concrete, ε is the strain and ε_c is the compressive strain.

To describe the post-cracking behavior of concrete in terms of its tensile characteristics, the fracture energy cracking criterion GFI was utilized. This criterion requires inputting the mean tensile strength f_{ctm} and fracture energy G_f in accordance with the recommendations outlined in the CEB-FIP model code [36] (Eq. 3).

$$G_f = G_{f0}\left(\frac{f_{cm}}{10}\right)^{0.7}, \tag{3}$$

where f_{cm} is the mean compressive concrete strength and G_{f0} is the base value of fracture energy, which depends on the size of the maximum aggregate in the concrete.

The CFRP strips and rods were modeled as an elastic isotropic brittle material until the ultimate tensile stress is reached, at which point brittle damage occurs. This modeling approach was adopted due to the unidirectional nature of the composite material, with primary stress applied in the fiber direction. The elastic modulus and ultimate strength of the CFRP bars used in the analysis are listed in Table 2. Additionally, a Poisson's ratio of 0.3 was assumed for the CFRP material.

The steel reinforcement was modeled using the elastic-plastic approach. The elastic modulus, yielding strength, and ultimate strength of the steel bars were determined through experimental testing, as discussed in Section 2.1. A Poisson's ratio of 0.3 was applied to the steel reinforcement in the analysis.

The epoxy-resin material was characterized by an elastic perfectly plastic stress-strain relationship. The values for the tensile resistance and modulus of elasticity of the resin can be found in Table 2. Additionally, a Poisson's ratio of 0.35 was adopted.

3.3 Interactions modeling

3.3.1 Interaction between concrete and steel rebars

Accurately representing the bond-slip behavior between the concrete and the embedded steel reinforcement is crucial to achieve distinct discrete crack patterns in the simulated beam model and realistic flexural responses beyond the cracking stage. In the current FE analyses, the bond between the longitudinal reinforcement and the concrete was simulated using 0-length SPRING2 elements, (nonlinear springs). These elements connect the concrete and steel elements at shared nodes, and the bond-slip relationship specified in the fib Model Code [36] was applied as follows:

$$\tau_b = \begin{cases} \tau_{b\max}(s/s_1)^{\alpha} & for\ s \le s_1 \\ \tau_{b\max} & for\ s_1 \le s \le s_2 \\ \tau_{b\max} - \dfrac{(\tau_{b\max} - \tau_{bf})(s - s_2)}{(s_3 - s_2)} & for\ s_2 \le s \le s_3 \\ \tau_{bf} & for\ s < s_3 \end{cases} \quad (4)$$

where, $\tau_{b\max} = 2.5\sqrt{f_{cm}}$, $\tau_{bf} = 0.4\ \tau_{b\max}$, $S_1 = 1.0$ mm, $S_2 = 2.0$ mm, S_3= distance between rebar ribs, and τ_b is the bond stress.

The discrete node-to-node connections used to simulate the bond-slip behavior necessitate the derivation of the bond force F instead of the bond stress τb, this relationship is expressed by Eq (5).

$$F = \tau_b c_r l_b, \quad (5)$$

where c_r is the circumference of the steel rebar, and l_b represents the bond length.

3.3.2 Interface between concrete and FRP

To simulate the bond behavior of the CFRP-adhesive-concrete connections, two layers of cohesive elements with a traction-separation model were used, one for the concrete/adhesive interface and the other for the CFRP-adhesive interface these elements behave in a linear elastic way until a damage initiation criterion is reached, followed by the propagation of damage which eventually leads to the degradation of the elements and failure of the bonded interface. The Quadratic Delamination criterion was adopted for the damage imitation with normal tress equal to the concrete tensile strength. The slip model developed by Zhang. [37], was adopted to calculate the maximum shear stress and the damage evolution in terms of fracture energy is given by the following equations:

$$G_f = 0.4\gamma^{0.422} f_c^{0.619}, \quad (6)$$

$$\tau_{\max} = 1.15\gamma^{0.138} f_c^{0.613}, \quad (7)$$

where $\tau_{\max}$ is the maximum shear stress, γ is the ratio of height to width for the grooves, f_c is the concrete compressive strength and G_f is the fracture energy.

4 Results and discussion

A comparison between experimental and numerical results is presented in Table 4, which summarizes the cracking load (P_{cr}), yield load (P_y), ultimate load (P_u), yield deflection (Δy), maximum deflection (Δu), and failure modes for the tested beams. The numerical results were obtained by simulating the tested beams using a finite element model as described in the previous section. The comparison shows good agreement between the experimental and numerical results, validating the accuracy of the proposed numerical model. The load-carrying capacity results indicate that the numerical values are slightly higher than the experimental ones, but the overall difference between the two sets of results is within an acceptable range.

Both control samples (c10 and c30) exhibited similar behavior, with beam c10 showing a higher peak load and deflection of approximately 27.26% and 10%, respectively, compared to beam c30 due to the lower concrete cover depth. A negligible increase in the cracking load of about 12%, 11%, 6.3%, and 1.2% for beams B30RF1, B10SF2, B30SF1, and B10SP1, respectively, was observed in comparison with the control beams. The yield load increased by 61%, 58%, 27.5%, and 21% respectively, for beams B30RF1, B30SF1, B10SF2, and B10SP1, due to the increased flexural stiffness during the second phase of the beam's behavior.

The use of NSM CFRP laminates significantly increased the ultimate load-carrying capacity of the RC beams. An increase of 69%, 70%, 39%, and 17% was obtained in

Table 4 Test results

Beam ID	Cracking load P_{cr} (kN)		Yield load P_y (kN)		Yield displacement Δy (mm)		Ultimate loads P_u (kN)		Ultimate displacement Δu (mm)		CFRP Strain at ultimate load (%)		μ	FM
	EXP	FEA	EXP	FEA	EXP	FEA	EXP	FEA	EXP	FEA	EXP	FEA		
C10	9.12	9.35	31.50	33.60	5.44	5.81	35.01	35.90	18.15	19.15	-	-	3.34	FF
C30	8.98	9.06	24.36	26.20	6.20	5.89	27.51	26.86	16.5	15.50	-	-	2.66	FF
B30RF1	10.08	10.21	39.37	38.39	4.60	4.72	46.46	47.18	6.34	6.45	0.35	0.35	1.37	ED + CDC
B30SF1	9.55	9.82	38.65	37.16	4.55	4.06	46.86	46.51	5.80	5.94	0.26	0.27	1.27	ED + CDC
B10SP1	9.25	9.67	34.78	36.45	4.61	4.52	40.41	40.95	5.40	5.68	0.38	0.38	1.17	ED + CDC
B10SF2	10.12	10.39	39.78	40.71	4.44	4.23	48.55	48.79	6.50	6.20	0.24	0.25	1.46	ED + CDC

Note: P_{cr} : cracking load, P_y and Δy: yielding and deflection load, P_u and Δu: ultimate load and deflection, μ (ductility index): $\Delta y/\ \Delta u$,
FM: Failure mode (FF: Flexural failure, ED: End debonding of the CFRP reinforcement, CDC: Critical diagonal crack)

terms of maximum load for B30SF1, B30RF1, B10SF2, and B10SP1, respectively, compared to the maximum load of the reference beam. Specimen B10SF1 had the highest peak load of 48.79 kN, indicating that cutting the bottom arm of the steel stirrups had negligible influence on the load-carrying capacity of the beams. However, beams strengthened with partly inserted strips had the lowest increase in load-bearing capacity due to the reduced contacting surface and groove size. It should be noted that beams with higher concrete cover depth saw greater improvement from reinforcement, as the steel reinforcement is further away from the region of highest stress concentration, which is at the bottom of the beam. In such cases, NSM bars can be particularly advantageous, as they are inserted precisely in this region of high-stress concentration, providing additional reinforcement and increasing the load-carrying capacity of the beam. However, the overall maximum load did not increase as much after the yielding load due to the onset of premature debonding failure modes that occurred in the strengthened beams, caused by the detachment of the concrete cover, resulting in a brittle failure mode. This ultimately limited the maximum load that the beam could support. A noticeable reduction in deflection at maximum load was observed in the NSM strengthened beams by 70.24%, 64.18%, 64.1%, and 61.6%, for specimens B10SP1, B10SF2, B30SF1, and B30RF1, respectively. This reduction can be explained by the observed failure mode of the CFRP bars, which was confirmed by the decrease in the ductility of the NSM strengthened beams defined as the ratio of ultimate deflection to yield deflection by 65%, 56.3%, 52.25%, and 48.5%, for beam B10SP1, B10SF2, B30SF1, and B30RF1, respectively. These results indicate that the use of NSM CFRP laminates can significantly increase the load carrying capacity of RC beams, but the design and installation should be carefully considered to prevent premature failure and ensure the long-term effectiveness of the reinforcement.

4.1 Load–deflection relationship

Fig. 5 presents the experimental and numerical load-deflection curves, which validate the reliability of the established predictive model. The behavior of CFRP strengthened beams resulted in a brittle failure mode, while the control beam exhibited more ductile behavior. The curves follow a three-phase response, characterized by concrete cracking, steel yielding, and post-yielding stages. Before cracking, the strengthened beams showed linear elastic behavior similar to the control beam in the first stage. The stiffness of the load-deflection curves was minimally impacted by NSM bars, and their effect on cracking behavior was slight due to the high flexural rigidity of beams and the bonding between the filling material and concrete not being affected yet. During the second stage, from cracking to steel yielding, the NSM bars increased the stiffness of the specimen and the yielding load compared to the control beam. Concrete cracking started in the beam cross-sections located in the maximum moment zone. Initially, the cracks did not cross the resin due to its low elastic modulus. As the load increased, the cracks widened, and new flexural cracks emerged. Cracking occurred uniformly throughout the beam length following the applied bending moment. Once the moment reached a value that caused the steel bars to yield, the concrete cracking stabilized. In the final stage, as the load increased, the deflection rate accelerated more rapidly than in the previous stage. Throughout this stage, the width of the cracks was controlled by the FRP bars until the point of failure was reached. The control beam experienced flexural failure, whereas the CFRP bar-strengthened beams experienced premature debonding, which significantly affected their reinforcement potential. Further analysis was conducted on the parameters governing the behavior of NSM FRP systems, which will be discussed in the following section.

4.2 Load–strain relationship

Fig. 6 shows good predictive accuracy of the variation in tensile strains in the CFRP reinforcement. It was observed that during the initial cracking stage, the CFRP bars had negligible load-carrying capacity, as their strains were almost zero. As a result, their contribution to enhancing the cracking load of the NSM-CFRP strengthened beams was minimal. However, as the load increased, the CFRP strain curves showed reasonable inclinations, indicating that the additional bars started to carry substantial loads, leading to a significant improvement in the yielding and ultimate loads of the beams.it can be seen that the CFRP strains displayed almost linear curves up to the tension steel yielding load, indicating that the CFRP bars effectively resisted the tensile stresses induced by the applied loads. After the tension steel yielded, the CFRP strains gradually increased up to the point of failure. This behavior of the CFRP bars during the loading process highlights their potential for enhancing the structural performance of reinforced concrete beams.

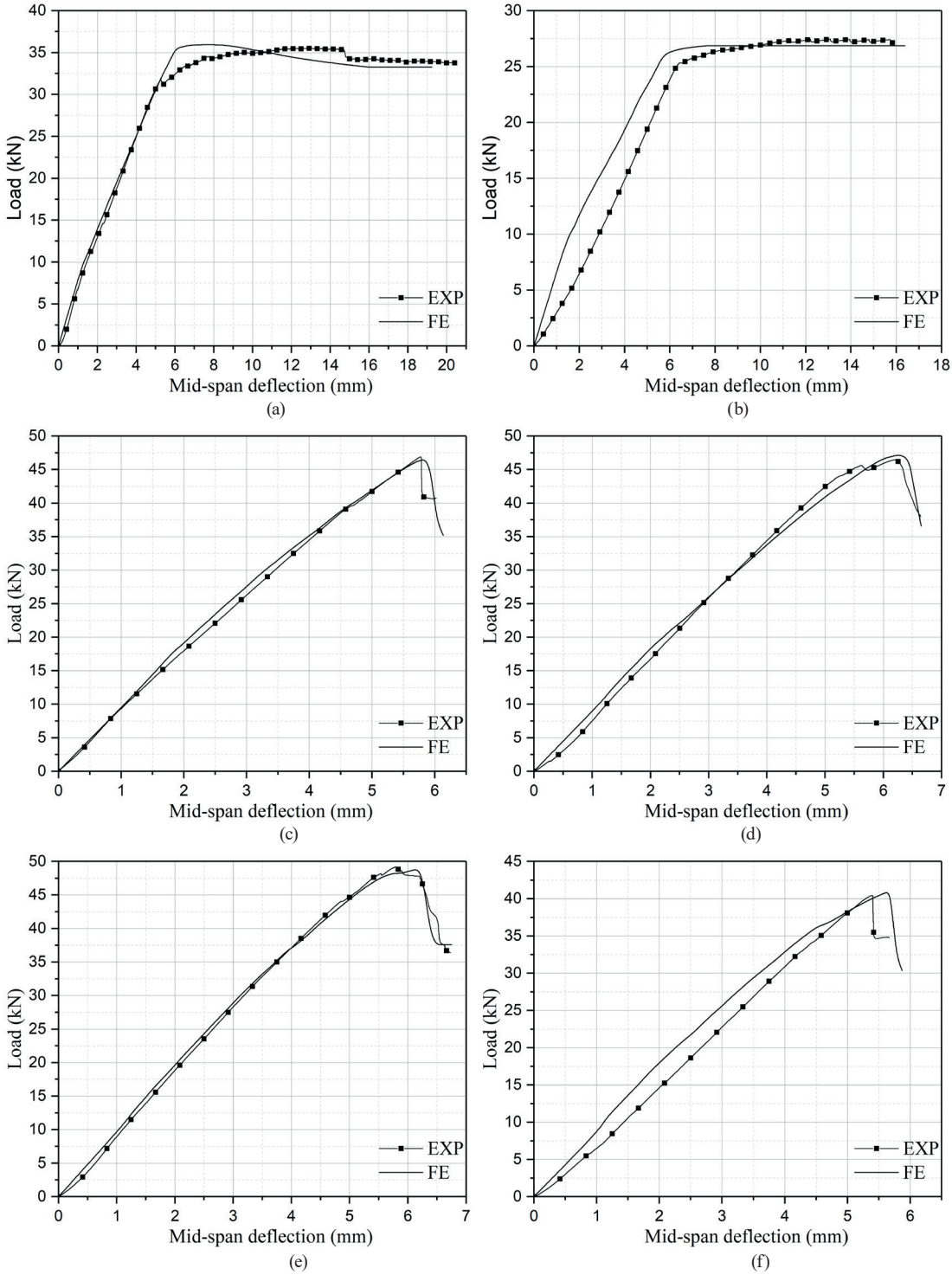

Fig. 5 Load-deflection curves for the tested specimens (a) REF (C10), (b) REF (C30), (c) B30SF1, (d) B30RF1, (e) B10SF1, (f) B10SP1

However, it should be noted that the maximum strain reached by the CFRP bars was only about 28% of their ultimate strain, indicating insufficient exploitation of the reinforcement potential. This was mainly due to the premature detachment of the reinforcement, which limited its effectiveness in improving the load-carrying capacity of the beams. Further improvements in the bonding between the CFRP bars and the concrete substrate are necessary to fully exploit the potential of NSM-CFRP reinforcement.

4.3 Failure modes

The crack pattern on the reference beam is illustrated in Fig. 7, which consisted of flexural cracks. The first cracks started from the mid-span on the tension side of the beam

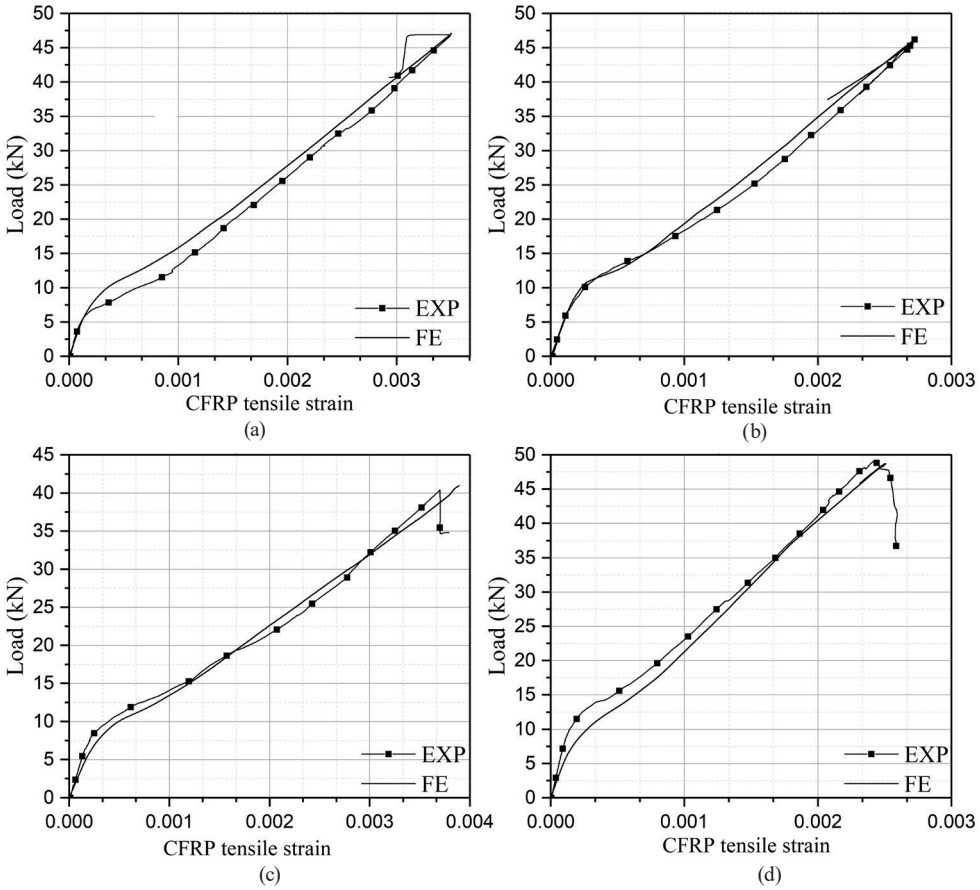

Fig. 6 Tension strain diagram on CFRP reinforcements (a) B30SF1, (b) B30RF1, (c) B10SP1, (c) B10SF1

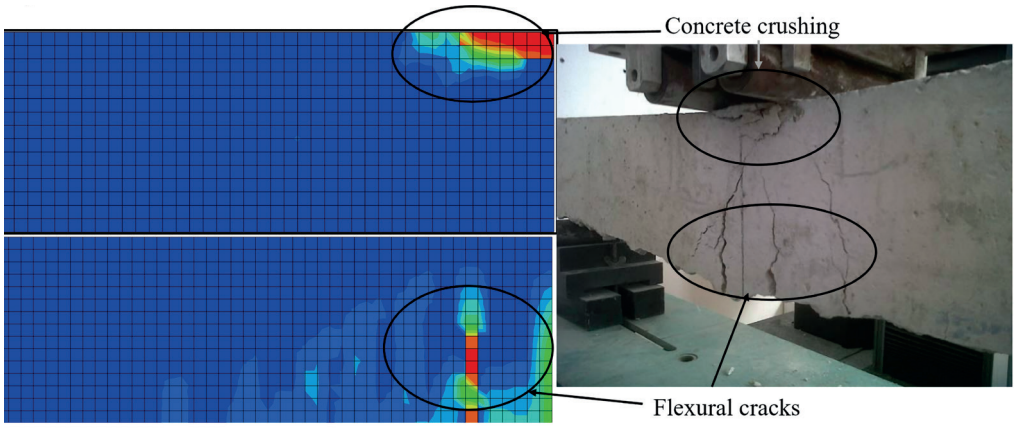

Fig. 7 Crack patterns and Failure modes of the reference beam: (a) C30 FEA, (b) C30 EXP

and propagated towards the neutral axis. Concrete crushing in the compression zone near the loading plates after the yielding of the tensile steel followed this. These observations indicate a flexural failure, which was accurately captured by the numerical model.

Fig. 8 presents the experimental recorded and numerically predicted failure modes and crack patterns of the beam strengthened with NSM CFRP strips. It was observed that the failure initiated with the end debonding of the CFRP strip from the bottom of the concrete beam sample, followed by a critical diagonal crack that started exactly from the end of the plate. This confirms the interaction between different failure phenomena close to the end of the FRP plate. The debonding failure mechanism of this set of beams was particularly influenced by the length of CFRP bars. The debonding failure was sudden and complete, occurring immediately after the yielding of the tension steel followed by a subsequent beam failure.

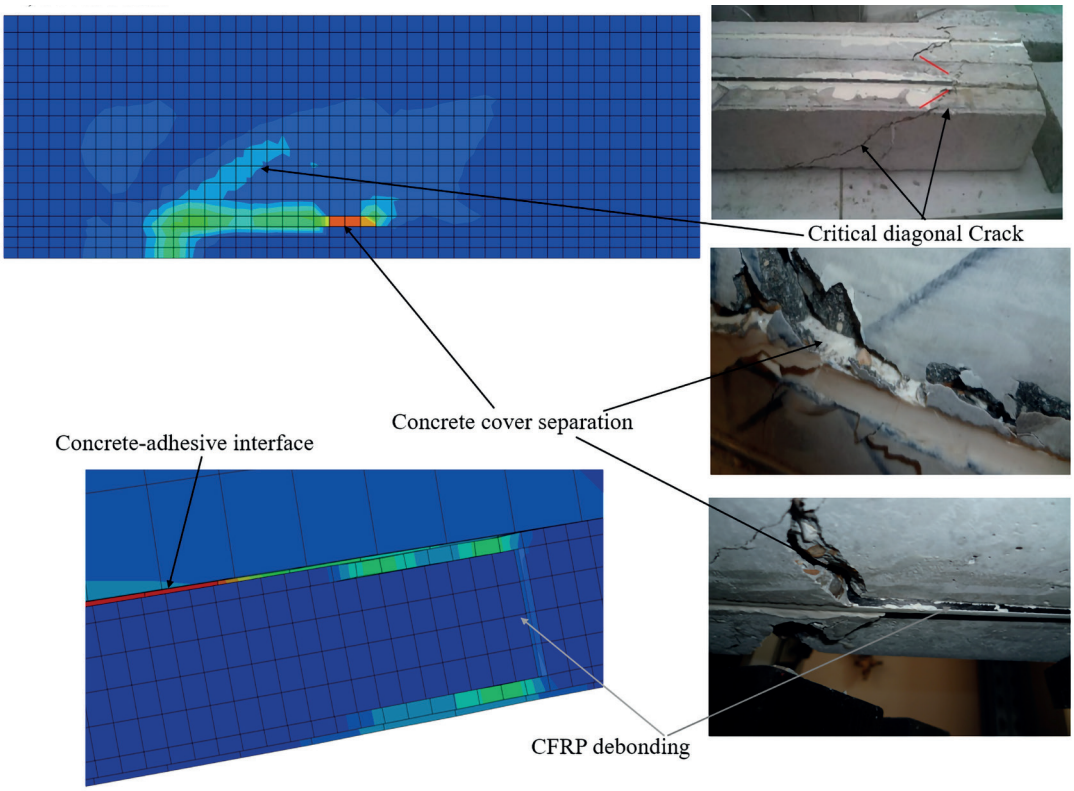

Fig. 8 Crack patterns and Failure modes of the NSM reinforced beams: (a) B30SF1 FEA, (b) B30SF1 EXP

5 Parametric studies

The validated FE model is used in this section to conduct a series of parametric stud into the effects of key variables affecting the behavior of NSM FRP strengthened RC beams.

5.1 Effect of the bond length and FRP bar number

This section explores the impact of the number of strips on a constant CFRP cross-sectional area and different embedment lengths. The reference strip dimensions, groove sizes, and spacing were the same as the experimental ones for comparison purposes.

Two concrete cover values (10 mm and 30 mm) were used, and the effect of 1, 2, 3, and 4 strips inserted within four different bond lengths (25%, 50%, 75%, and 100% of the beam span) was considered. Load-deflection curves were produced for the different cases, and their mechanical characteristics in terms of cracking load, yield load, ultimate load, yield displacement, ultimate displacement, ductility, and failure modes were evaluated and summarized in Table 5, showing a detailed illustration of the effect of the number of strips in conjunction with the effect of bond length on different mechanical characteristics. An overall increase in cracking and yielding load was observed when the number of strips increased for all tested bond lengths, which can be attributed to the increased stiffness of the beams. Fig. 9 shows the effect of varying the NSM bar number for different reinforcement lengths. It is clear that for a bond length of 25% L, the influence of NSM bars on the load capacity was marginal, regardless of bar number and concrete cover. Increasing the bond length to 50% L resulted in an increase of (27.52%, 41.20%, 52.95%, 45.26%) and (59.72%, 79.37%, 104.54%, 87.53%) for a bar number equal to 1, 2, 3, and 4 and concrete cover of 10 mm and 30 mm, respectively, compared with the control beam. In the case of a bond length of 75% L, an increase of (36.3%, 73.06%, 86.99%, 69.83%) and (68.02%, 120.44%, 142.29%, 124.35%) for a bar number equal to 1, 2, 3, and 4 and concrete cover of 10 mm and 30 mm, respectively, was recorded, comparing with the control beam. The highest increase was recorded when using a bond length of 100%, resulting in (107.99%, 109.89%, 112.34%, 101.45%) and (138.61%, 151.71%, 180.53%, 174.01%) for bar number 1, 2, 3, and 4 and concrete cover of 10 mm and 30 mm, respectively, in comparison with the concrete beam. It should be noted that this increase was not proportional to the increase in the number of bars. For a bond length of 100%, using two NSM bars resulted in a negligible increase of 1% and 5% for concrete covers

Table 5 FE analysis results for various NSM bar number and lengths

Beam ID	Concrete COVER	CFRP length	*N*	P_{cr} (kN)	P_y (kN)	Δy (mm)	P_u (kN)	Δu (mm)	P_u (%)	μ	FM
C10 (CB)	10	/	/	9.35	33.60	5.81	35.90	19.10	/	3.29	FF
B10N1L25	10	0.25 L	1	9.39	40.67	4.38	39.32	6.10	9.53	1.39	ED
B10N2L25			2	9.41	37.11	4.07	43.26	5.65	20.50	1.39	ED
B10N3L25			3	9.60	38.04	4.03	43.43	6.31	20.97	1.57	ED
B10N4L25			4	10.21	39.63	4.23	43.61	8.25	21.48	1.95	ED
B10N1L50	10	0.50 L	1	9.77	41.70	4.60	45.78	6.51	27.52	1.41	ED
B10N2L50			2	9.90	41.58	4.05	50.69	8.20	41.20	2.02	ED
B10N3L50			3	10.21	49.20	4.40	54.91	9.05	52.95	2.06	ED + CDC
B10N4L50			4	10.95	42.16	4.72	52.15	8.36	45.26	1.77	ED + CDC
B10N1L75	10	0.75 L	1	10.39	39.78	4.23	48.93	5.91	36.30	1.40	ED + CDC
B10N2L75			2	10.61	51.72	4.35	62.13	9.59	73.06	2.47	ED + CDC
B10N3L75			3	10.71	57.54	4.77	67.13	8.58	86.99	1.78	CCS
B10N4L75			4	11.01	52.64	4.87	60.97	7.97	69.83	1.64	CCS
B10N1L100	10	L	1	10.85	55.80	5.11	74.67	13.08	107.99	2.55	FF + ICD
B10N2L100			2	11.41	64.09	4.60	75.35	11.64	109.89	2.53	FF+ICD
B10N3L100			3	12.48	71.13	4.45	76.29	8.32	112.34	1.87	SF
B10N4L100			4	12.68	70.34	4.22	72.35	7.54	101.45	1.79	SF
C30 (CB)	30	/	/	9.06	26.20	5.89	26.86	16.39	/	2.78	FF
B30N1L25	30	0.25 L	1	9.15	35.71	4.64	39.14	5.80	45.72	1.25	ED
B30N2L25			2	9.35	37.03	4.26	39.29	5.29	46.28	1.24	ED
B30N3L25			3	9.71	38.06	4.91	42.15	8.08	56.92	1.65	ED
B30N4L25			4	10.11	32.07	4.27	42.45	8.10	58.04	1.90	ED
B30N1L50	30	0.50 L	1	9.27	38.93	4.41	42.90	6.22	59.72	1.41	ED
B30N2L50			2	9.82	44.10	4.79	48.18	9.21	79.37	1.92	ED
B30N3L50			3	10.31	49.01	4.86	54.94	8.41	104.54	1.73	ED+CDC
B30N4L50			4	10.92	58.42	4.60	50.37	7.51	87.53	1.63	ED+CDC
B30N1L75	30	0.75 L	1	9.82	37.16	4.06	45.13	5.85	68.02	1.44	ED
B30N2L75			2	10.51	49.88	4.53	59.21	8.80	120.44	1.94	ED
B30N3L75			3	10.81	54.11	4.22	65.08	7.61	142.29	1.80	CCS
B30N4L75			4	11.38	54.04	4.19	60.26	7.32	124.35	1.74	CCS
B30N1L100	30	L	1	10.09	50.57	5.23	64.09	12.45	138.61	2.38	FF+ICD
B30N2L100			2	11.12	57.02	4.79	67.61	12.37	151.71	2.58	FF+ICD
B30N3L100			3	12.08	61.65	4.35	75.37	10.75	180.53	2.47	SF
B30N4L100			4	13.35	70.35	4.50	73.60	7.61	174.01	1.69	SF

Note: L: Beam span, N: Number of CFRP bars , P_{cr}: cracking load, P_y and Δy: yielding and deflection load, P_u and Δu: ultimate load and deflection, Pu% is the percentage increase in the load carrying capacity in comparison with the control beam, μ (ductility index): $\Delta y/\Delta u$, FM is the failure mode (FF: Flexural failure, ED: FRP end debonding, CDC: Critical diagonal crack, CCS: Concrete cover separation, ICD: Intermediate crack debonding, SF: Shear failure)

of 30 mm and 10 mm, respectively. Increasing the number of bars to four resulted in a reduction of the load capacity of the beams, which can be explained by the weakened concrete cover because of the larger grooves area and the interference between the NSM bars. In this case, the failure mode changed from a ductile to shear failure, significantly compromising the strength of the beam.

Fig. 10 depicts the ductility index variation concerning different NSM bar numbers and lengths. The same trend was observed for beams with concrete cover of 10 and 30 mm. The results showed that bond length had the most significant impact on ductility. For a single NSM bar, increasing the CFRP bar length from 75% L to 100% L led to a ductility increase of approximately 82% and 65% for beams with

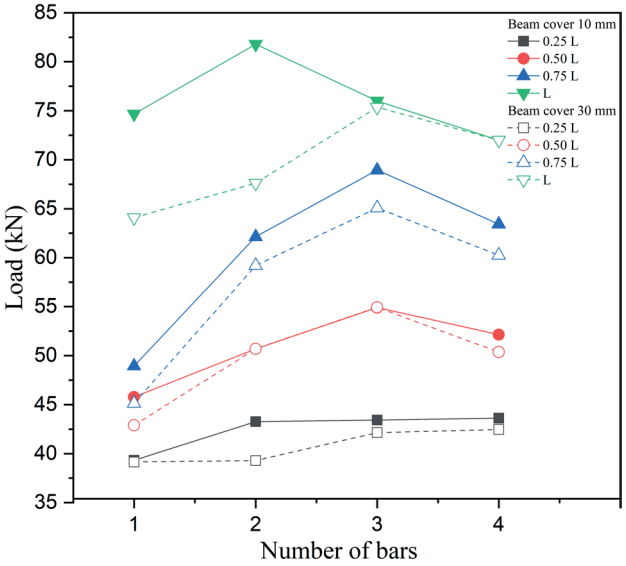

Fig. 9 The effect of NSM bar length and number

concrete covers of 30 mm and 10 mm, respectively. This change also altered the beam's failure mode from a premature debonding to a more ductile flexural and intermediate crack debonding failure. In the case of two NSM bars, an 8% increase in ductility was noted for the concrete cover of 30 mm, while it had a negligible effect on the lower concrete cover. However, increasing the bar number from 2 to 4 resulted in a significant decrease in ductility of approximately 29% for both concrete cover lengths and changed the failure mode to brittle shear failure.

Moreover, it was observed that using two NSM bars with lengths of 50% and 75% resulted in a significant increase in ductility of approximately 43% and 76% for concrete covers of 10 mm and 30 mm, respectively, compared to using one bar. However, this increase was nullified when the number of bars was increased further.

5.2 Effect of the concrete strength and FRP Type

The influence of concrete strength on NSM bars made of four different FRP materials (CFRP, AFRP, BFRP and GFRP) was investigated. Four different concrete grades (25 MPa, 35 MPa, 45 MPa, and 65 MPa) were explored. A single NSM bar with a bond length of 100% L was used.

Results are summarized in Table 6.

The properties of CFRP strips were provided in the experimental study and typical mechanical properties found in the literature [38] were used for the AFRP, BFRP, and GFRP strips and are listed in Table 7. Control beams were tested for each concrete grade, and bond-slip model parameters were calculated using Eq. (6) and Eq. (7). The results indicated an overall increase in beam characteristics as the concrete strength increased.

The load-deflection curves for the tested specimens showed trilinear behavior, with all strengthened beams exhibiting an almost similar trend at all loading stages and increased load capacity compared to the non-strengthened beam. The curves showed an approximate trilinear response, characterized by concrete cracking, steel yielding, and post-yielding stages as shown in Fig. 11. All the composites showed similar performance, with CFRP reinforced beams exhibiting superiority as the concrete strength increased. For beams strengthened with AFRP, GFRP, and BFRP, greater displacement was observed in lower concrete strengths due to their higher elongation. As the concrete grade increased to 45 MPa, the failure mode of the beams strengthened with GFRP bars changed to FRP rupture, with the strains in the composites reaching the ultimate value, resulting in beam failure. This failure mode was also observed for beams reinforced with BFRP and AFRP bars when the concrete was 65 MPa.

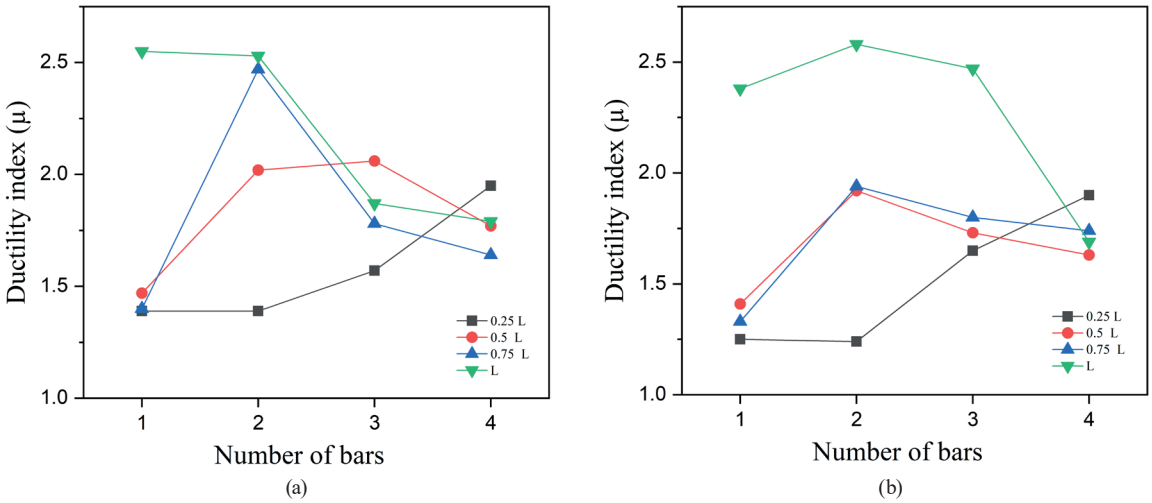

Fig. 10 Effect of NSM bar length and number on the ductility index (a) Concrete over 10 mm, (b) Concrete over 30 mm

Table 6 FE analysis results for various concrete grades and FRP material types

Beam ID	f_c	Material type	P_{cr} (kN)	P_y (kN)	Δy (mm)	P_u (kN)	Δu (mm)	P_u (%)	μ	FM
C10-25 (CB)	25	/	9.05	33.73	5.79	34.07	15.87	/	2.74	FF
B10-CFRP25		CFRP	10.32	54.41	5.13	62.93	11.64	84.71	2.27	ICD
B10-AFRP25		AFRP	9.88	47.79	5.12	60.51	15.64	77.60	3.05	ICD
B10-BFRP25		BFRP	9.45	47.46	5.13	60.12	16.55	76.46	3.23	ICD
B10-GFRP25		GFRP	9.37	46.96	5.14	59.38	16.97	74.29	3.3	ICD
C10-35 (CB)	35	/	9.35	33.60	5.85	35.90	19.10	/	3.26	FF
B10-CFRP35		CFRP	10.85	55.80	5.11	74.67	13.08	107.99	2.55	ICD
B10-AFRP35		AFRP	10.27	49.64	4.58	64.99	17.39	82.20	3.8	ICD
B10-BFRP35		BFRP	9.48	49.38	4.80	63.72	16.36	78.64	3.41	ICD
B10-GFRP35		GFRP	9.44	47.42	4.45	62.70	17.12	75.78	3.85	ICD
C10-45 (CB)	45	/	15.60	37.46	4.43	39.74	19.74	/	4.46	FF
B10-CFRP45		CFRP	17.36	63.54	4.79	83.44	11.95	111.40	2.49	ICD
B10-AFRP45		AFRP	16.92	52.10	4.26	73.87	17.64	87.15	4.14	ICD
B10-BFRP45		BFRP	16.87	51.61	4.53	71.58	17.57	81.35	3.88	ICD
B10-GFRP45		GFRP	16.79	50.68	4.54	68.27	14.26	72.97	3.14	FR
C10-65 (CB)	65	/	18.91	39.40	4.22	44.16	19.59	/	4.64	FF
B10-CFRP65		CFRP	22.02	63.38	4.15	96.88	14.30	119.38	3.45	FF
B10-AFRP65		AFRP	20.88	51.79	3.97	80.57	17.05	82.45	4.29	FR
B10-BFRP65		BFRP	20.84	51.13	3.98	78.92	15.14	78.71	3.8	FR
B10-GFRP65		GFRP	20.75	50.33	3.99	73.66	13.64	66.80	3.42	FR

Note: f_c: concrete strength, P_{cr}: cracking load, P_y and Δy: yielding and deflection load, P_u and Δu: ultimate load and deflection, P_u% is the percentage increase in the load carrying capacity in comparison with the control beam, μ (ductility index): $\Delta y/\Delta u$, FM is the failure mode (FF: Flexural failure, ICD: Intermediate crack debonding, FR: FRP rupture)

Table 7 Material properties of FRP materials

	AFRP	BFRP	GFRP
Tensile strength (MPa)	1300	1100	900
Modulus of elasticity (GPa)	59	55	48
Ultimate strain (%)	1.93	1.45	1.69

In contrast, no FRP rupture occurred in beams strengthened with CFRP bars due to its higher mechanical characteristics. The ultimate load for the various materials and concretes was presented in Fig. 12. The increase in concrete strength resulted in an increase in the ultimate load of beams strengthened with all the composites used. CFRP reinforced beams had a higher percentage increase in ultimate load compared to the other composites, but this came at the expense of ductility for lower concrete strengths due to concrete brittle failure. AFRP strengthened beams had the highest ductility for high concrete grade, while GFRP bars performed best at lower grade concrete, as shown in Fig. 13.

In summary, AFRP, GFRP, and BFRP are more cost-effective and better suited for low-strength concrete, while CFRP is more suitable for high-strength concrete grades.

5.3 Effect of FRP reinforcement ratio

This section aimed to investigate the effect of different reinforcement ratios on the performance of NSM FRP bars using a constant bar length of 100% L. In addition to the original CFRP cross-sectional area of 50 mm^2 used in the previous sections, two values of 25 mm^2 and 12.5 mm^{2}were examined in this section for a different number of bars, and the results are summarized in Table 8. Given that the previous sections had already covered specimens with a cross-sectional area of 50 mm^2, which resulted in a change of the failure mode to shear due to over-reinforcing, as illustrated in Fig. 14, they were not further discussed in this section. Fig. 15 depicts the load-deflection curves of the tested beams, showing that the curves generally exhibit similar behavior with increased ductility when the cross-section of the bar decreased. In general, beams strengthened with distributed smaller cross-sectional area NSM bars performed better than beams strengthened with higher ones for similar reinforcement ratios, indicating the importance of determining the optimal positioning for maximum efficacy and stress distribution. Fig. 16 demonstrates the effect of the CFRP cross-sectional area

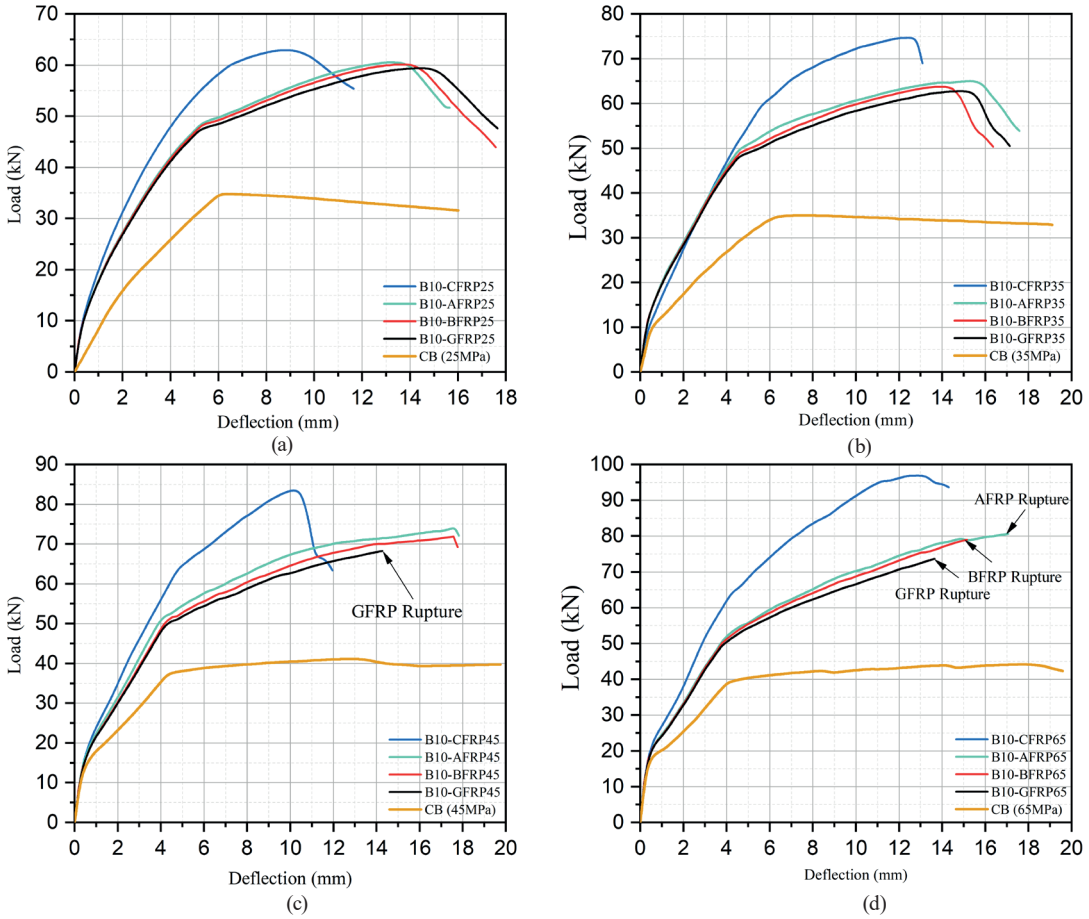

Fig. 11 Load-deflection curve for various materials: a) *f*c 25 MPa, b) *f*c 35 MPa, c) *f*c 45 MPa, d) *f*c 65 MPa

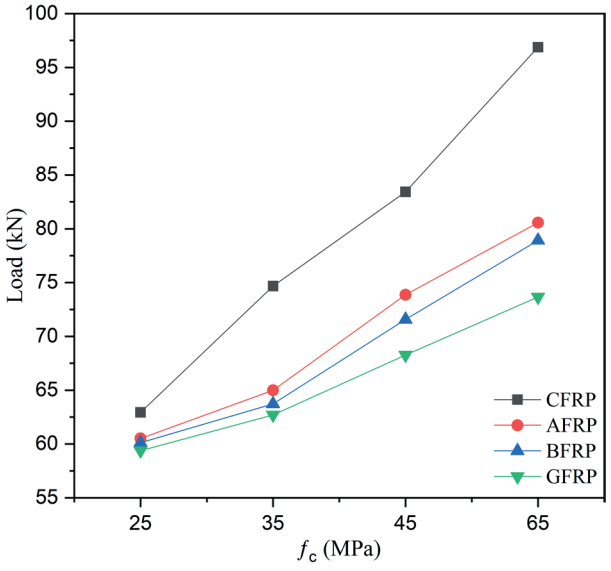

Fig. 12 Effect of the concrete strength for different FRP materials

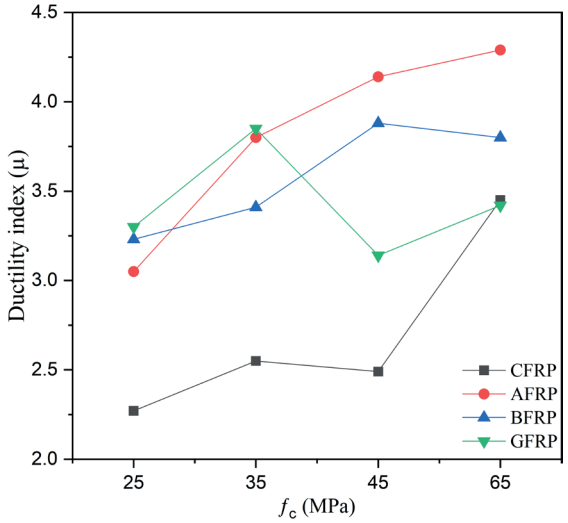

Fig. 13 Effect of the concrete strength for different FRP materials on the ductility index

for different numbers of NSM bars, showing that increasing the number of bars while using smaller cross-sectional area leads to a higher ultimate load. Fig. 17 shows the influence of the reinforcement cross-section on the ductility of the beams, with a significant increase in ductility of about 63% observed in the case of using 2 bars of 12.5 mm^2 sectional area instead of one bar at 25 mm^2, even though they had the same reinforcement ratio of 0.167%. This is because the use of smaller section bars results in a uniform distribution of loads and a more gradual failure mode

Table 8 FE analysis results for various reinforcement ratios

ID	CS (mm^2)	N	P_{cf} (%)	P_{cr} (kN)	P_y (kN)	Δy (mm)	P_u (kN)	Δu (mm)	P_u %	μ	FM
B10N1L100-CS1	50	1	0.33	10.85	55.80	5.11	74.67	13.08	107.99	2.55	FF + ICD
B10N2L100-CS1		2	0.67	11.41	64.09	4.60	75.35	11.64	109.89	2.53	FF + ICD
B10N3L100-CS1		3	1	12.48	71.13	4.45	76.29	8.32	112.34	1.87	SF
B10N4L100-CS1		4	1.33	12.68	70.34	4.22	72.35	7.54	101.45	1.79	SF
B10N1L100-CS2	25	1	0.167	10.54	50.22	5.03	66.80	13.21	86.07	2.63	FF + ICD
B10N2L100-CS2		2	0.33	11.21	57.54	5.22	77.58	16.48	116.10	3.16	FF + ICD
B10N3L100-CS2		3	0.50	11.68	65.38	5.25	81.52	13.99	127.08	2.66	ICD
B10N4L100-CS2		4	0.67	14.11	70.43	5.45	80.91	13.70	125.38	2.51	ICD
B10N1L100-CS3	12.5	1	0.083	9.94	45.06	4.74	60.50	14.08	68.52	2.97	ED
B10N2L100-CS3		2	0.167	10.61	48.30	4.83	73.32	20.78	104.23	4.30	FF + ICD
B10N3L100-CS3		3	0.25	12.77	53.67	4.85	81.15	19.06	126.04	3.93	FF + ICD
B10N4L100-CS3		4	0.33	13.34	57.88	5.06	79.71	18.66	122.03	3.69	FF

Note: CS is cross-sectional area of the CFRP bars, N is the number of CFRP bars, P_{cf} is the percentage of (cross-sectional area of the CFRP reinforcements / cross-sectional area of the beam), P_{cr}: cracking load, P_y and Δy: yielding and deflection load, P_u and Δu: ultimate load and deflection, P_u% is the percentage increase in the load carrying capacity in comparison with the control beam, μ (ductility index): $\Delta y/ \Delta u$, FM is the failure mode (FF: flexural failure ED: end debonding, ICD: Intermediate crack debonding, SF: Shear failure)

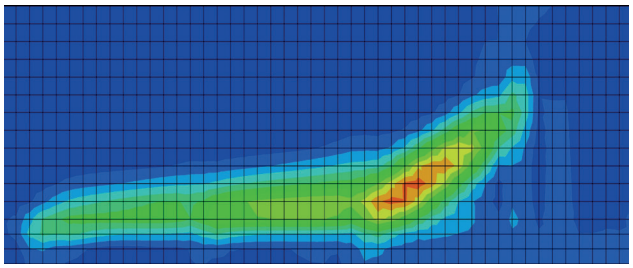

Fig. 14 Shear failure of the beam B10N4L100-CS1

compared to using one large area bar, which can lead to a sudden failure mode. This is especially evident for beams having low concrete cover. It is worth noting that increasing the number of bars may enhance the performance of the strengthened beams, but it also increases the complexity of installation and the cost of reinforcement. Hence, a balance between the cost and benefits of using a larger number of smaller bars versus using fewer larger bars is crucial for an optimal reinforcement strategy. This can

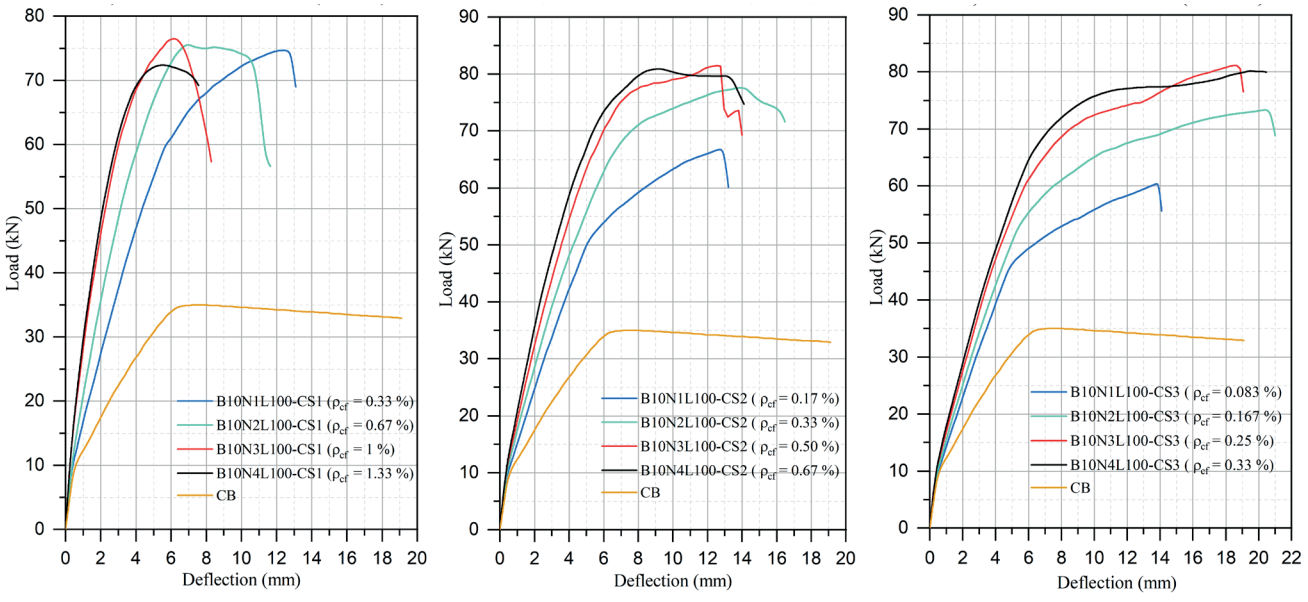

(a) (b) (c)

Fig. 15 load-deflection curve for various CFRP ratios and cross-sectional area (a) CFRP cross-sectional area (50 mm^2), (b) CFRP cross-sectional area (25 mm^2), (c) CFRP cross-sectional area (12.5 mm^2)

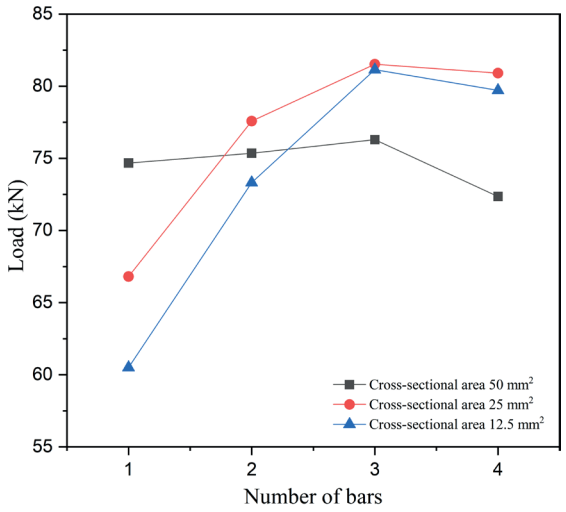

Fig. 16 Effect of the CFRP cross-sectional area for different number of NSM bars

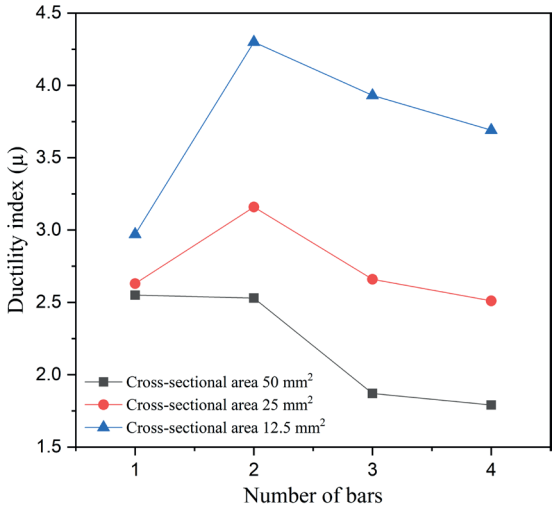

Fig. 17 Effect of the CFRP cross-sectional area for different number of NSM bars on the ductility index

be achieved by taking into account factors such as the required strength, ductility, and the expected durability of the reinforced beam.

5.4 Effect of FRP reinforcement method

In this section, the effect of bar positioning on the behavior of reinforced concrete beams was investigated using the side near-surface mounted (SNSM) technique.

The SNSM technique involves placing the FRP bars on 1the sides of the beams instead of at the bottom, as shown in Fig. 18. The study considered two concrete cover lengths of 10 mm and 30 mm and bond lengths ranging from 25% to 100% of the beam span. The results obtained from the study are summarized in Table 9.

Fig. 19 compares the load-deflection curves for NSM and SNSM techniques for different concrete cover and bond lengths. As discussed in the previous section, the beams

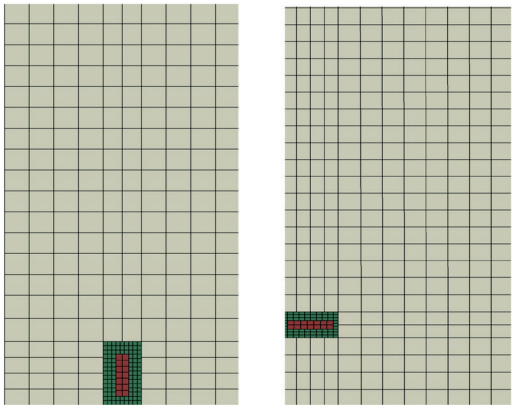

(a) (b)

Fig. 18 CFRP strip positioning for NSM and SNSM technique (a) Bottom mounted CFRP strip, (b) Side mounted CFRP strip

Table 9 FE analysis results for NSM and SNSM techniques

Beam ID	Concrete cover	CFRP length	P_{cr} (kN)	P_y (kN)	Δy (mm)	P_u (kN)	Δu (mm)	P_u %	μ	FM
C30 (CB)		/	9.06	26.20	5.89	26.86	16.39	/	2.78	FF
SNSM-B30L25		0.25 L	11.12	35.67	4.55	38.41	6.12	43.00	1.34	ED
SNSM-B30L50	30	050 L	11.97	36.76	4.01	48.14	6.93	79.23	1.73	ED + CDC
SNSM-B30L75		0.75 L	12.36	44.34	4.86	55.30	12.72	105.88	2.62	CCS
SNSM-B30L100		L	12.43	48.32	5.04	59.75	15.75	122.45	3.13	ICD
C10 (CB)		/	9.35	33.60	5.81	35.90	19.10	/	3.29	FF
SNSM-B10L25		0.25 L	11.81	39.80	4.24	41.74	6.07	16.27	1.26	ED
SNSM-B10L50	10	050 L	12.38	39.77	4.25	53.54	8.85	49.14	2.08	ED + CDS
SNSM-B10L75		0.75 L	12.54	43.87	4.96	59.44	12.63	65.57	2.55	CCS
SNSM-B10L100		L	12.58	47.03	4.98	67.87	17.05	89.05	3.42	ICD

P_{cr}: cracking load, P_y and Δy: yielding and deflection load, P_u and Δu: ultimate load and deflection, P_u% is the percentage increase in the load carrying capacity in comparison with the control beam, μ (ductility index): $\Delta y/\Delta u$, FM is the failure mode (FF: Flexural failure, ED: FRP end debonding, CDC: Critical diagonal crack, CCS: Concrete cover separation, ICD: Intermediate crack debonding)

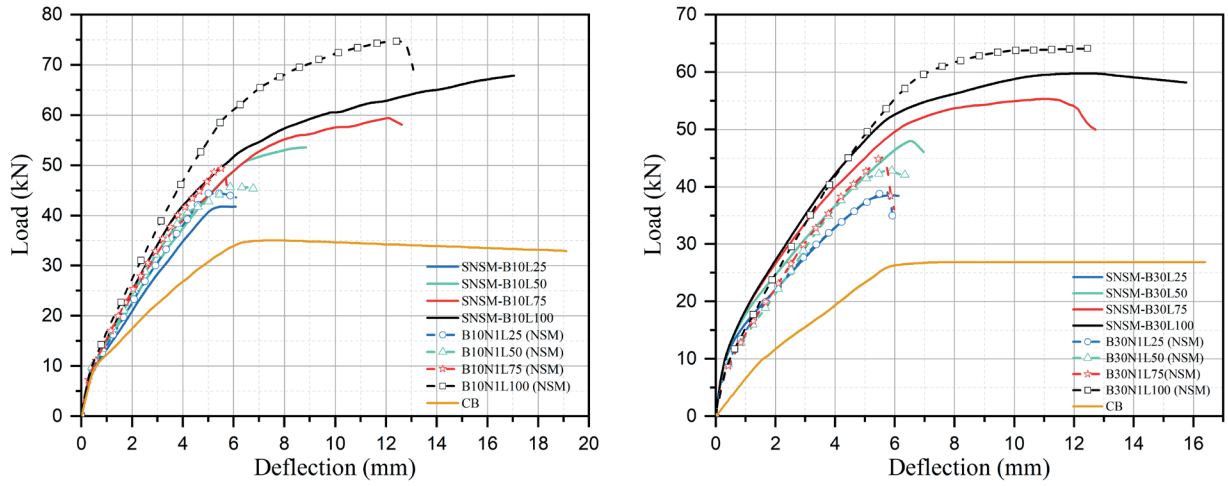

Fig. 19 Load-deflection curves for NSM and SNSM techniques (a) Concrete cover 10 mm, (b) Concrete cover 30 mm

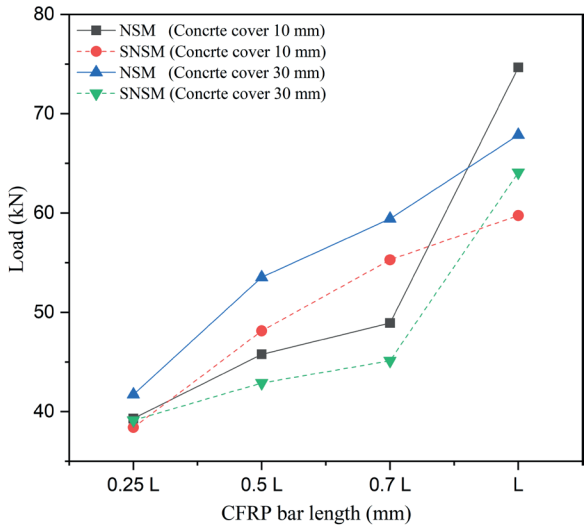

Fig. 20 Effect of different bar lengths for NSM and SNSM techniques

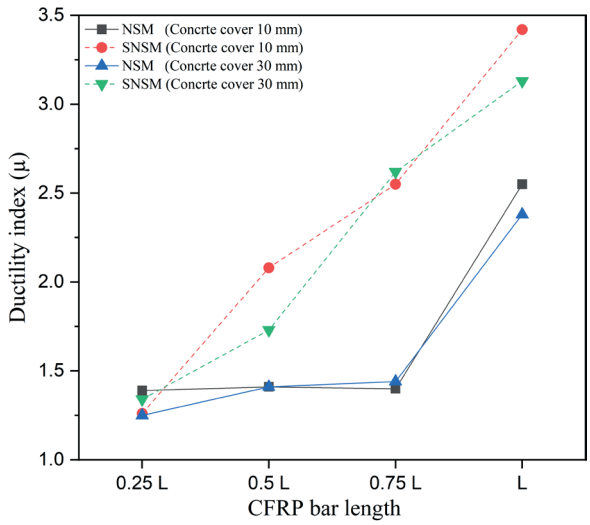

Fig. 21 ductility index for the NSM and SNSM technique

showed typical three-phase behavior, with the SNSM technique showing better ductile behavior than the NSM technique.

Fig. 20 shows a comparison of the ultimate load between NSM and SNSM techniques for different bond lengths. The most significant difference occurred for lower bond lengths, where the SNSM technique increased both the load and deflection in comparison with NSM. Interestingly, for a bond length equal to the beam span, NSM strengthened beams had better load-bearing capacity, while SNSM had more ductility with a slight decrease in resistance. This behavior is due to the bars being placed higher than the area of the highest stress.

Fig. 21 presents a detailed comparison of the ductility achieved by the NSM and SNSM techniques for different bond lengths. The results show that overall, the beams strengthened with the SNSM technique exhibited significantly better ductility performance than those strengthened with NSM, with improvements of (48%, 82%, and 34%) and (22%, 82%, and 32%) for bar lengths of (50% L, 75% L, and 100% L), and concrete covers of 10 mm and 30 mm, respectively in comparison with the NSM technique. It is worth noting that the highest ductility was achieved at the full bond length for both strengthening techniques. This can be attributed to the fact that in this case, the bars are able to develop their full bond strength, leading to a better transfer of forces between the concrete and the bars.

Overall, the results suggest that the SNSM technique is a more effective way to improve the ductility of reinforced concrete beams compared to NSM, especially when the bond length is relatively short.

6 Conclusions

The effectiveness of using NSM CFRP strip/rod for strengthening RC beams was investigated in this study using different strengthening techniques, such as partial inclusion of reinforcements, and fully inserted reinforcements with cut stirrups by performing an experimental investigation and developing a 3D nonlinear finite element model. The following conclusions can be drawn.

- Cutting the lower part of the steel stirrups to install the CFRP profiles has no effect on the ultimate load and the beam deformability.
- Strengthening reinforced concrete beams with NSM CFRP strips/rods increases significantly their load-bearing capacity.
- The numerical model was able to accurately predict the ultimate loads and the failure modes of the tested beams. The predicted results were in excellent correlation with the experimental ones.
- The Ductility was decreased in NSM-strengthened RC beams in comparison with the reference beams.
- Increasing the NSM bar length significantly enhances both the load-carrying capacity and ductility of the strengthened beams. This is particularly evident when extending the NSM bars to the full span of the beam.
- Using smaller cross-sectional area FRP bars with optimal positioning significantly improves the performance and ductility of reinforced concrete beams.
- An increase in beam characteristics was observed with an increase in concrete strength.
- CFRP reinforced beams exhibited the highest ultimate load increase, but lower ductility for low-strength concrete.
- AFRP, GFRP, and BFRP were found to be more cost-effective for low-strength concrete.
- CFRP was identified as the ideal choice for high-strength concrete.
- Debonding of the CFRP reinforcement was the most common failure mode in this study.
- The SNSM technique significantly improves the ductility of reinforced concrete beams compared to NSM, particularly for short bond lengths.
  Notably, the highest ductility was achieved when the bars were placed at full bond length for both techniques.

Acknowledgements

This investigation was conducted in the L2MGC Laboratory of Civil Engineering Department, Cergy Pontoise University (France). Polymer and epoxy materials.

References

[1] Al-Zahrani, M. M., Al-Dulaijan, S. U., Nanni, A., Bakis, C. E., Boothby, T. E. "Evaluation of bond using FRP rods with axisymmetric deformations", Construction and Building Materials, 13(6), pp. 299–309, 1999. https://doi.org/10.1016/s0950-0618(99)00038-0

[2] Leeming, M. B., Darby, J. J. "Design and specifications for FRP plate bonding of beams" In: Holloway, L. C., Leeming, M. (eds.) Strengthening of reinforced concrete structures, Woodhead Publishing, 1999, pp. 242–269. ISBN: 978-1-85573-378-7

[3] Lau, K. T., Dutta, P. K., Zhou, L. M., Hui, D. "Mechanics of bonds in an FRP bonded concrete beam", Composites Part B: Engineering, 32(6), pp. 491–502, 2001. https://doi.org/10.1016/s1359-8368(01)00032-4

[4] Quantrill, R. J., Hollaway, L. C., Thorne, A. M. "Experimental and analytical investigation of FRP strengthened beam response: Part I", Magazine of Concrete Research, 48(177), pp. 331–342, 1996. https://doi.org/10.1680/macr.1996.48.177.331

[5] Arduini, M., Nanni, A. "Behavior of Precracked RC Beams Strengthened with Carbon FRP Sheets", Journal of Composites for Construction, 1(2), pp. 63–70, 1997. https://doi.org/10.1061/(asce)1090-0268(1997)1:2(63)

[6] Lee, J. H., Lopez, M. M., Bakis, C. E. "Slip effects in reinforced concrete beams with mechanically fastened FRP strip", Cement and Concrete Composites, 31(7), pp. 496–504, 2009. https://doi.org/10.1016/j.cemconcomp.2009.04.008

[7] Barros, J. A. O., Dias, S. J. E., Lima, J. L. T. "Efficacy of CFRP-based techniques for the flexural and shear strengthening of concrete beams", Cement and Concrete Composites, 29(3), pp. 203–217, 2007. https://doi.org/10.1016/j.cemconcomp.2006.09.001

[8] Täljsten, B. "Strengthening concrete beams for shear with CFRP sheets", Construction and Building Materials, 17(1), pp. 15–26, 2003. https://doi.org/10.1016/s0950-0618(02)00088-0

[9] Meier, U., Deuring, M., Meier, H., Schwegler, G. "CFRP Bonded Sheets", In: Nanni, A. (ed.) Fiber-Reinforced-Plastic (FRP) Reinforcement for Concrete Structures, Elsevier, 1993, pp. 423–434. ISBN: 978-0-444-89689-6 https://doi.org/10.1016/b978-0-444-89689-6.50023-9

[10] Nanni, A. "North American design guidelines for concrete reinforcement and strengthening using FRP: principles, applications and unresolved issues", Construction and Building Materials, 17(6–7), pp. 439–446, 2003. https://doi.org/10.1016/s0950-0618(03)00042-4

[11] Limam, O., Foret, G., Ehrlacher, A. "RC two-way slabs strengthened with CFRP strips: experimental study and a limit analysis approach", Composite Structures, 60(4), pp. 467–471, 2003. https://doi.org/10.1016/s0263-8223(03)00011-4

[12] Van Den Einde, L., Zhao, L., Seible, F. "Use of FRP composites in civil structural applications", Construction and Building Materials, 17(6–7), pp. 389–403, 2003. https://doi.org/10.1016/s0950-0618(03)00040-0

[13] Teng, J. G., Smith, S. T., Yao, J., Chen, J. F. "Intermediate crack-induced debonding in RC beams and slabs", Construction and Building Materials, 17(6–7), pp. 447–462, 2003. https://doi.org/10.1016/s0950-0618(03)00043-6

[14] Merdas, A., Fiorio, B., Chikh, N.-E. "Étude de l'adhérence des joncs et des plats composite avec le béton par flexion (beam test)", (Study of the adhesion of composite strips and rods to concrete by bending), Comptes Rendus Mécanique, 339(12), pp. 796–804, 2011. (in French). https://doi.org/10.1016/j.crme.2011.10.002

[15] Merdas, A., Fiorio, B., Chikh, N.-E. "Aspects of bond behavior for concrete beam strengthened with carbon fibers reinforced polymers–near surface mounted", Journal of Reinforced Plastics and Composites, 34(6), pp. 463–478, 2015. https://doi.org/10.1177/0731684415573814

[16] Douadi, A., Merdas, A., Sadowski, Ł. "The bond of near-surface mounted reinforcement to low-strength concrete", Journal of Adhesion Science and Technology, 33(12), pp. 1320–1336, 2019. https://doi.org/10.1080/01694243.2019.1592944

[17] Sadoun, O., Merdas, A., Douadi, A. "The bond and flexural strengthening of reinforced concrete elements strengthened with near surface mounted prestressing steel (PS) bars", Journal of Adhesion Science and Technology, 34(19), pp. 2120–2143, 2020. https://doi.org/10.1080/01694243.2020.1753278

[18] Lundquist, J., Nordin, H., Täljsten, B., Olofsson, T. "Numerical analysis of concrete beams strengthened with CFRP: a study of anchorage lengths", In: Proceedings of the International Symposium on Bond Behaviour of FRP in Structures (BBFS 2005), Hong Kong, China, 2005, pp. 239–246. ISBN: 9623675062

[19] Vasquez, D., Seracino, R. "Assessment of the Predictive Performance of Existing Analytical Models for Debonding of Near-Surface Mounted FRP Strips", Advances in Structural Engineering, 13(2), pp. 299–308, 2010. https://doi.org/10.1260/1369-4332.13.2.299

[20] Barros, J. A. O., Varma, R. K., Sena-Cruz, J. M., Azevedo, A. F. M. "Near surface mounted CFRP strips for the flexural strengthening of RC columns: Experimental and numerical research", Engineering Structures, 30(12), pp. 3412–3425, 2008. https://doi.org/10.1016/j.engstruct.2008.05.019

[21] Obaidat, Y. T., Heyden, S., Dahlblom, O. "The effect of CFRP and CFRP/concrete interface models when modelling retrofitted RC beams with FEM", Composite Structures, 92, pp. 1391–1398, 2010. https://doi.org/10.1016/j.compstruct.2009.11.008

[22] Hawileh, R. A. "Nonlinear finite element modeling of RC beams strengthened with NSM FRP rods", Construction and Building Materials, 27(1), pp. 461–471, 2012. https://doi.org/10.1016/j.conbuildmat.2011.07.018

[23] Rezazadeh, M., Cholostiakow, S., Kotynia, R., Barros, J. "Exploring new NSM reinforcements for the flexural strengthening of RC beams: Experimental and numerical research", Composite Structures, 141, pp. 132–145, 2016. https://doi.org/10.1016/j.compstruct.2016.01.033

[24] Hosen, M. A., Jumaat, M. Z., Islam, A. B. M. S. "Side Near Surface Mounted (SNSM) technique for flexural enhancement of RC beams", Materials & Design, 83, pp. 587–597, 2015. https://doi.org/10.1016/j.matdes.2015.06.035

[25] Movahedi Rad, M., Khaleel Ibrahim, S., Lógó, J. "Limit design of reinforced concrete haunched beams by the control of the residual plastic deformation", Structures, 39, pp. 987–996, 2022. https://doi.org/10.1016/j.istruc.2022.03.080

[26] Khaleel Ibrahim, S., Movahedi Rad, M. "Reliability-based probabilistic numerical plastically limited analysis of reinforced concrete haunched beams", Scientific Reports, 13(1), 2670, 2023. https://doi.org/10.1038/s41598-023-29930-0

[27] Khaleel Ibrahim, S., Movahedi Rad, M. "Limited Optimal Plastic Behavior of RC Beams Strengthened by Carbon Fiber Polymers Using Reliability-Based Design", Polymers, 15(3), 569, 2023. https://doi.org/10.3390/polym15030569

[28] Szép, J., Habashneh, M., Lógó, J., Movahedi Rad, M. "Reliability Assessment of Reinforced Concrete Beams under Elevated Temperatures: A Probabilistic Approach Using Finite Element and Physical Models", Sustainability, 15(7), 6077, 2023. https://doi.org/10.3390/su15076077

[29] NF "NF P18-406 Essai de compression [Compression test]", French Standardization Association, Paris, France, 1981. (in French)

[30] NF "NF P18-408 Essai de traction [Tensile test]", French Standardization Association, Paris, France, 1981. (in French)

[31] EN " EN 10002-1:2001 Metallic materials - Tensile testing - Part 1: Method of test at ambient temperature", European Committee for Standardization, Brussels, Belgium, 2001.

[32] ISO " ISO 527-1:2012 Plastics – Determination of tensile properties – Part 1: General principles", International Organization for Standardization, Geneva, Switzerland, 2012.

[33] ISO "ISO-527-2:2012 Plastics – determination of tensile properties – part 2: test conditions for moulding and extrusion plastics", international Organization for Standardization, Geneva, Switzerland, 2012.

[34] ABAQUS "Analysis User's Manual, Version 6.14", [online] Available at: http://130.149.89.49:2080/v6.14/index.html [Accessed: 7 July 2022]

[35] Carreira, D. J., Chu, K.-H. "Stress-Strain Relationship for Plain Concrete in Compression ", ACI Journal Proceedings, 82(6), pp. 797–804, 1985. https://doi.org/10.14359/10390

[36] Fib "Model Code 2010-Final draft: Volume 1", International Federation for Structural Concrete, Lausanne, Switzerland, 2012.

[37] Zhang, S. S., Teng, J. G., Yu, T. "Bond–slip model for CFRP strips near-surface mounted to concrete", Engineering Structures, 56, pp. 945–953, 2013. https://doi.org/10.1016/j.engstruct.2013.05.032

[38] Aydın, E., Boru, E., Aydın, F. "Effects of FRP bar type and fiber reinforced concrete on the flexural behavior of hybrid beams", Construction and Building Materials, 279, pp. 122–407, 2021. https://doi.org/10.1016/j.conbuildmat.2021.122407